Available online at www.sciencedirect.com
ScienceDirect
Biomaterials 28 (2007) 271–284
Biomaterials
www.elsevier.com/locate/biomaterials

Immobilized nerve growth factor and microtopography have distinct effects on polarization versus axon elongation in hippocampal cells in culture

Natalia Gomez[a], Yi Lu[b], Shaochen Chen[b,d,e], Christine E. Schmidt[a,c,d,e,*]

[a]*Department of Chemical Engineering, The University of Texas at Austin, Austin, TX 78712 1062, USA*
[b]*Department of Mechanical Engineering, The University of Texas at Austin, Austin, TX 78712 1062, USA*
[c]*Department of Biomedical Engineering, The University of Texas at Austin, Austin, TX 78712 1062, USA*
[d]*Texas Materials Institute, The University of Texas at Austin, Austin, TX 78712 1062, USA*
[e]*Center for Nano- and Molecular Science and Technology, The University of Texas at Austin, Austin, TX 78712 1062, USA*

Received 4 April 2006; accepted 25 July 2006
Available online 17 August 2006

Abstract

Cell interfacing with biomaterial surfaces dictates important aspects of cell behavior. In particular, axon extension in neurons is effectively influenced by surface properties, both for the initial formation of an axon as well as for the maintenance of axon growth. Here, we investigated how neurons behaved on poly(dimethyl siloxane) (PDMS) surfaces decorated with biochemical and physical cues presented individually or in combination. In particular, nerve growth factor (NGF) was covalently tethered to PDMS to create a bioactive surface, and microtopography was introduced to the material in the form of microchannels. Embryonic hippocampal neurons were used to investigate the impact of these surface cues on polarization (i.e., axon initiation or axogenesis) and overall axon length. We found that topography had a more pronounced effect on polarization (68% increase over controls) compared to immobilized NGF (0.1 ng/mm^2) (27% increase). However, the effect of NGF was negligible when both types of stimuli were simultaneously presented on the biomaterial surface. In addition to axon formation, chemical and physical cues are also involved in axon growth following the initiation process. Interestingly, for the same studies described above, the effects of microchannels and NGF were opposite from the effects on polarization; the most evident effect was for the immobilized growth factor (10% increase in axon length with respect to controls) whereas there was no effect in general for the microtopography. More importantly, when the two surface stimuli were presented in combination, a synergistic increase in axon length was detected (25% increase with respect to controls), which could be a result of faster polarization triggered by topography plus enhanced growth from NGF. Additionally, axon orientation was also analyzed and we found the well-known tendency of perpendicular or parallel axonal alignment to be dependent on the width and depth of the channels. This investigation thoroughly compared and distinguished the individual and combined impact of material surface properties (chemical and physical) on axogenesis from the effects on axon length. Overall, topography dominated polarization mechanisms, whereas NGF, and particularly a synergy of immobilized NGF plus topography, dominated axon length. These results could be potentially applied for the design of biomaterials in applications were axon growth is critical.
© 2006 Elsevier Ltd. All rights reserved.

Keywords: Polarization; Axon growth; Hippocampal neurons; Contact guidance; Nerve growth factor

1. Introduction

Interfaces between engineered materials and cells play a critical role in biomedical applications where the interaction between cells and the material surface dictates cell performance and therefore, the success of the implanted device. Extracellular matrix (ECM) components and

*Corresponding author. Department of Chemical Engineering, The University of Texas at Austin, Austin, TX 78712 1062, USA.
Tel.: +1 512 471 1690; fax: +1 512 471 7060.
E-mail address: schmidt@che.utexas.edu (C.E. Schmidt).

0142-9612/$ - see front matter © 2006 Elsevier Ltd. All rights reserved.
doi:10.1016/j.biomaterials.2006.07.043

peptides, topographical features, support cells and growth factors [1–4] have been extensively studied for the creation of biomimetic materials that control cellular responses such as adhesion, morphology or differentiation. More recently, combinations of such environmental cues have proven to be advantageous for targeting multiple aspects of cell behavior and improving cell responses in applications such as osteogenesis [5,6], nerve regeneration [7–9], and endothelialization [10].

With respect to neural engineering applications, patterned adhesive areas [15–17], contact guidance cues [18–20], delivery of nerve growth factors [21,22] and electrically conductive substrates [23] have been particularly used with the goal of improving axon regeneration after trauma [13,14]. However, whether these stimuli influence axon formation, axon elongation or both has not been extensively studied. In this study, we have focused on understanding the effect of environmental cues on axon initiation versus overall axon elongation. We also explored if different types of stimuli, such as chemical ligands that bind to specific receptors, or physical signals that are transduced by cytoskeleton tension, could preferentially affect one of these processes. We directly compared neuron responses to two different cues that were presented either individually or in combination. Immobilized NGF was used as the model chemical ligand, whereas surface microtopography in the form of microchannels was investigated as the physical stimulus. These studies were performed presenting the cues as surface properties of a designed material, which could be adapted for neural engineering applications to better design biomaterials that modulate neuron responses. For example, biomaterials used in nerve guidance conduits could be modified to present both topographical features and immobilized NGF to enhance nerve regeneration.

Physical guidance, also called contact guidance, has been recognized as a guidance mechanism for neurons for many years [11]. Observations in developmental studies have acknowledged the presence of natural physical cues provided by glial cells to migrating neurons in the central nervous system [24,25]. In an attempt to mimic such signals, artificial substrata have been designed with microstructures, generally microchannels (i.e., ridges and grooves) that stimulate neurons to grow aligned along the channels. A wide range of patterns effectively influence neurite orientation and length. Specifically, depths between 15 nm and 4 μm, and widths ranging from 1 to 25 μm have been shown to influence both alignment [18,26–28] and growth rate of neurites [27,29].

In addition to physical cues, chemical ligands such as growth factors are potent modulators of cell responses. Neurotrophins, a family of growth factors, have been investigated extensively because of trophic and chemotactic effects, in addition to their roles in cell survival and differentiation [30–32]. NGF is the most studied and characterized neurotrophin, known for inducing several neuron responses, including neurite outgrowth. Although some of NGF's effects require endocytosis of the ligand–receptor complex [32], neurite outgrowth is not necessarily mediated by retrograde transport [33,38–40] and possibly controlled by localized actin polymerization [34]. Thus, NGF immobilized to substrata is effective in inducing neurite extension, turning and sprouting [35–40]. Other growth factors including insulin, epidermal growth factor and vascular endothelial growth factor have also been immobilized in active form on a variety of substrates [41–43]. A common approach for this protein immobilization is the use of arylazido-containing compounds, which can react nonspecifically with UV light by creating singlet nitrenes that undergo insertion into C–H, N–H and other bonds [44,45]. Using this method, proteins have been fixed to many substrates such as poly(vinyl alcohol), polystyrene, poly(ethylene terephthalate), and chitosan [41,42,46–49].

To better study axon formation responses to surface stimuli, embryonic hippocampal neurons were used because these cells are the most common and best-characterized model for investigating polarization [12,50]. Polarization of these neurons occurs spontaneously in culture during the first 48–72 h, during which the neurons follow very well-defined stages, from stage 1 where cells are unpolarized, to stage 3 where the cells establish an axon [50,51]. Numerous studies have focused on understanding the underlying mechanisms that determine this polarization phenomenon from similar growing neurites, and major molecules such as Cdc42, PIP_3, GSK-3β and PAR-3 have been identified as playing a critical role [52–55]. The majority of these investigations have focused on the identification of intracellular pathways that determine polarization in the absence of external signals. The environmental signals that can effectively influence polarization have been studied to a lesser extent. Biochemical cues such as laminin [56] and NGF [57] increase the number of hippocampal cells in stage 3 (i.e., polarized cells) during the first 24 h in culture. Additionally, physical cues such as tension [58] and topographical features [59] also influence the directionality or rate of polarization. However, combination of contact guidance and immobilized growth factors has not been explored before for polarization and axon elongation in neurons.

Here we describe our efforts to investigate how surface properties influence the rate of polarization and axon length of hippocampal cells. In particular, we studied the combination of two different material surface properties: topographical characteristics that provide contact guidance and biochemical signals. To provide these two signals, microchannels of 1–2 μm in width were microfabricated on PDMS, a biocompatible, inexpensive and commonly used material in soft lithography applications, which allowed us to obtain multiple substrates by simple replica molding of the polymer. NGF was subsequently immobilized on these microstructures to create a bioactive surface. We found that the two stimuli could individually increase the percentage of neurons in stage 3 (i.e., *initiation effect*) after

20 h in culture with a more drastic effect for the topography, but there was no additive effect on initiation when both cues were present simultaneously. Additionally, these cues also increased axon length (i.e., *elongation effect*), with a more pronounced impact for the immobilized NGF and a synergistic increase for the simultaneous stimuli. We also found that microtopography affected the *orientation* of axon growth by producing larger axonal alignment when deeper and wider microchannels were present, which is consistent with previous reports.

2. Materials and methods

2.1. Microfabrication of channels

Microchannels 1 and 2 μm wide and 400 and 800 nm deep were created on PDMS using soft lithography techniques. The procedure consisted of three steps: (1) fabrication of a mask with the desired patterns, (2) fabrication of a silicon master, and (3) replica molding of the PDMS.

The mask was created with electron beam (E-beam) lithography. Four-μm-thick low-temperature oxide was initially deposited on a silicon wafer (WaferWorld, West Palm Beach, FL) using low-pressure chemical vapor deposition (LPCVD). The wafer was then annealed at 1000 °C for 1 h to enhance film density and etching durability. The wafers were subsequently cut into 1 cm^2 pieces and cleaned by sonication in acetone, isopropyl alcohol and water. 4% poly(methyl methacrylate) PMMA resist in chlorobenzene (Microchem, Newton, MA) was spin coated for 45 s and 3000 rpm, and baked for 30 min at 170 °C. Microchannels of 1 or 2 μm were written on the PMMA resist using E-beam (Raith-50 and XL-30 SEM, LaB_6 source) with an area dose of 220 $\mu As/cm^2$ and beam current of 0.2 nA. After the patterns were written, the exposed areas were developed with a mixture of methyl-isobutyl-ketone and isopropyl alcohol (1:3) (Sigma, St. Louis, MO) for 1.5 min.

After the microchannels were written with E-beam, the next step was thermal evaporation (Denton) of a 100 nm chromium (R.D. Mathis, Long Beach, CA) film and lift-off with acetone, which created a Cr mask on the silicon substrate. Reactive ion etching (RIE) of the SiO_2 layer was performed in an etcher (Plasma Technology) with a mixture of CHF_3 and oxygen until the desired thickness was obtained and measured with a Nanospec (Nanometrics). The Cr-coated areas were wet-etched with a mixture of ceric sulfate and nitric acid (Transene, Danvers, MA) for 2 min. The final master was silanized with tridecafluoro-1,1,2,2-(tetrahydrooctyl) trichlorosilane (Gelest, Morrisville, PA).

The microchannels on PDMS were produced by pouring a mixture of Sylgard 184 (Dow Corning, Midland, MI) on the master (one part curing agent per 10 parts base), curing for 24 h at room temperature and releasing the film. This step was performed multiple times for a single master.

2.2. NGF-FITC conjugation

NGF was conjugated to fluorescein for detection and characterization of the immobilization procedure. 40 μL of sodium bicarbonate buffer (0.1 M, pH = 9) was mixed with 100 μL of NGF 2.5S (Promega, Madison, WI, 100 μg/mL) and 10 μL of fluorescein isothiocyanate in dimethyl sulfoxide (FITC, 12 mg/mL) (Molecular Probes, Carlsbad, CA). The reaction was carried out at 4 °C for 10 h. The unreacted FITC was separated by centrifugation using size exclusion chromatography columns (Biorad, Hercules, CA, exclusion limit 6000 Da). Conjugation efficiency and degree of labeling were evaluated with a UV-Vis Beckman DU500 spectrophotometer by measuring absorbance at 280 and 494 nm. NGF-FITC was only used for quantification and visualization purposes, but not for cell culture because some loss of activity was detected in PC12 cell neurite extension assays (results not shown).

A calibration curve of NGF standards was obtained by casting known quantities of the fluorescent protein on defined areas without washing, calculating surface concentrations (ng/mm^2) and capturing fluorescence images of the dry samples with a fluorescence microscope (IX-70, Olympus) using a constant exposure time. Before analysis, standards were exposed to UV light for 15 s (this was the exposure time for immobilizing NGF in the experiments), to take into account any loss of fluorescence as a result of photobleaching. For all hippocampal cell culture, unlabeled NGF was used at the same concentrations as used for NGF-FITC experiments.

2.3. NGF immobilization

NGF photochemical fixation was performed using a phenyl-azido group, a method developed by Matsuda et al. [42] and modified by Ito and colleagues for immobilization of growth factors in particular [37,38,43]. The procedure consisted of three main steps (Fig. 1): (1) preparation of *N*-4-(azidobenzoyloxy)succinimide according to a previously published procedure [42]; (2) polyallylamine (PAA) conjugation to N-4-(azidobenzoyloxy)succinimide, and (3) fixation of NGF using the modified polyallylamine. Briefly, *N*-4-(azidobenzoyloxy)succinimide was obtained by adding a solution of dicyclohexylcarbodiimide (Aldrich, St. Louis, MO) (6.7 g) in tetrahydrofuran (25 mL) to a solution of *N*-hydroxysuccinimide (Aldrich) (3.7 g) and 4-azidobenzoic acid (TCI America, Portland, OR) (4.8 g) in tetrahydrofuran (75 mL), followed by filtration and crystallization with isopropyl alcohol/diisopropyl ether (Aldrich). Subsequently, a solution of 15 mg of polyallylamine (Aldrich) in 10 mL of phosphate buffered saline (PBS, pH = 7.4) was added to a solution of 13 mg of *N*-4-(azidobenzoyloxy)succinimide in 5 mL of *N*,*N*-dimethylformamide and stirred for 24 h at 4 °C. The solution was ultrafiltered (10,000 Da NMWL; Millipore, Billerica, MA) and washed three more times by adding 10 mL of distilled-deionized (DDI) water and ultrafiltered again to finally obtain a volume of ~300 μL of photosensitive polyallylamine (PAA-Azido).

The conjugate was analyzed by measuring UV-Vis absorbance of the filtration retentate at 280 nm. This conjugate was diluted in DDI water to obtain a final volume of 1.2 mL (1:4). A 50 μL aliquot of this solution was cast on a PDMS substrate (1 cm^2), air dried and exposed with a UV lamp (Blak-Ray, 22 mW/cm^2, $\lambda_{max} = 365$ nm) for 15 s followed by three washes with 0.05 M HCl and two washes with PBS. This step was followed by casting a second layer of the photosensitive polyallylamine (50 μL) and a superimposed final layer of NGF (for cell culture) or NGF-FITC (for quantification) (1–2 μg in 50 μL of PBS). For controls, PBS only was added instead of NGF solution, which produced a PDMS substrate only immobilized with PAA-azido. Finally, the substrate was exposed to UV light for 15 s and washed six times with PBS to remove unreacted protein and then rinsed two more times with DDI water.

To illustrate the versatility of the immobilization procedure, patterning experiments were performed as proof of principle for future applications. A TEM grid (Electron Microscopy Sciences) was placed on top of the dried layers before UV exposure to serve as a mask. Also, instead of using the UV lamp a solid-state Nd:YAG laser (Surelite, Continuum) with a wavelength of 355 nm was used to create gradients of NGF on the surface by focusing and scanning lines with different exposure times. The substrate was placed on top of an automated stage, and the exposure time was controlled by the scanning rate. A laser energy of 6 μJ was used with stage speeds between 20 and 180 μm/s.

2.4. NGF ELISA assay

An ELISA assay was performed to determine how much NGF was released from the surface. PDMS substrates with immobilized NGF ($n = 3$) were placed in 3 cm tissue culture dishes and incubated in PBS for 3 days at 37 °C. Volumes of 200 μL were collected from the dishes at 6, 24, 48, and 72 h and analyzed with a commercially available sandwich ELISA kit (NGF E_{max} kit, Promega). Briefly, 96-well ELISA plates were coated with a primary goat anti-NGF antibody overnight at 4 °C, followed by incubation with blocking buffer (1 h) and incubations of samples and standards for 6 h at room temperature. Finally, a secondary rat anti-NGF

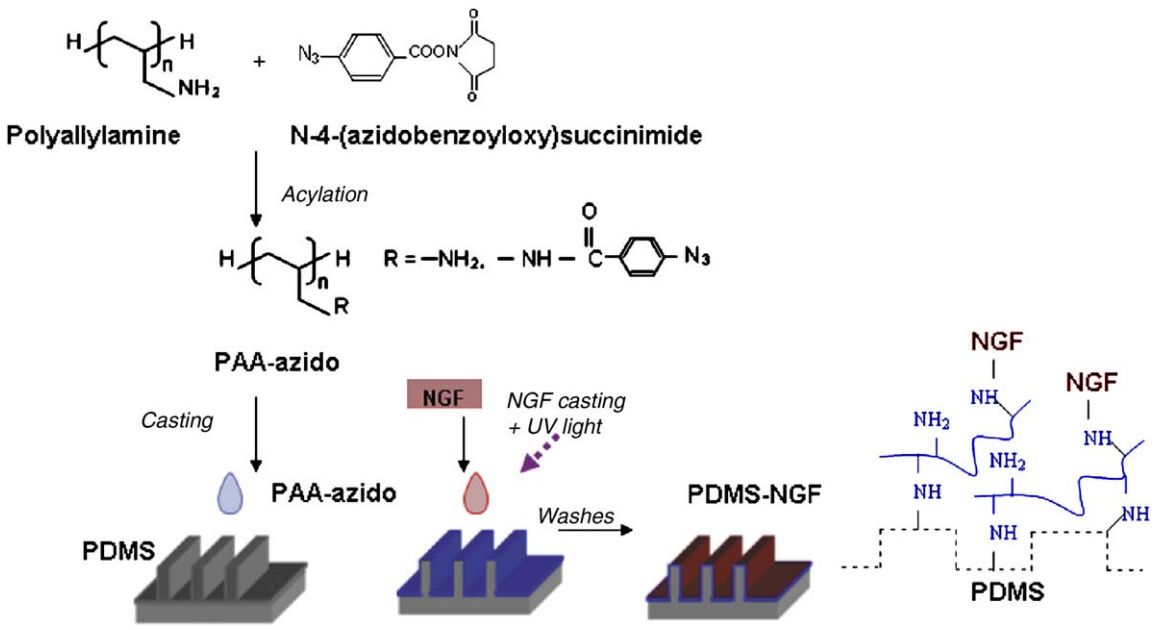

Fig. 1. Schematic of the NGF immobilization process. PAA was conjugated to an azido compound to produce PAA-azido. This conjugate was cast twice on PDMS, followed by casting of NGF. UV light exposure promoted the formation of covalent bonds via the azido groups, immobilizing NGF to PDMS.

antibody was incubated overnight, followed by incubation with anti-rat antibody conjugated to horseradish peroxidase (HRP) for 2.5 h, and development with 3,3′,5,5′-tetramethylbenzidine (TMB). HCl 1 M was added to all wells, and absorbance at 450 nm was recorded using a plate reader.

2.5. Hippocampal cell culture

For cell culture, treated PDMS substrates were subsequently transferred to sterile 3 cm tissue culture dishes, washed twice with sterile water, air dried and stored at 4 °C. Embryonic rat hippocampal cells (E18) were isolated from commercially obtained hippocampus tissue (BrainBits, Springfield, IL). The hippocampi were incubated with papain (Worthington, Lakewood, NJ) in Hibernate E medium (BrainBits) (4 mg/mL) at 30 °C for 20 min, followed by physical trituration with a fire-polished Pasteur pipette. Cells were counted and plated on already prepared PDMS substrates (7.5×10^3 cells/cm^2), and cultured with Neurobasal Medium (Invitrogen, Carlsbad, CA) supplemented with 2% B-27 (Invitrogen), L-glutamine (Fisher, 0.5 mM), L-glutamic acid (Sigma, 25 μM) and 1% antibiotic-antimycotic (Sigma, 10,000 units/mL of penicillin, 10 mg/mL of streptomycin and 25 μg/mL of amphotericin).

Cells were incubated on different substrates including PDMS with immobilized NGF and PDMS with PAA-azido and microchannels. Negative controls were PDMS with PAA-azido only. Positive controls included PDMS with PAA-azido and NGF in solution (10–50 ng/mL) and laminin-coated PDMS (incubation overnight at 4 °C with 10 μg/mL). Laminin was used as a positive control because of its well-known effect on polarization [56].

2.6. Immunochemistry

After 20 h in culture at 37 °C and 5% CO_2, cells were fixed with 4% paraformaldehyde (Sigma), 4% sucrose (Fisher) in PBS for 20 min, followed by permeabilization for 20 min with 0.1% Triton-X100 (Sigma) in 2% bovine serum albumin (BSA) (Jackson ImmunoResearch, West Grove, PA) in PBS, and blocking for 1 h at 37 °C with 2% BSA-PBS. Samples were incubated with antibodies for Tau-1 (axonal marker) (Chemicon, Temecula, CA, 1:200) and NGF (Abcam, Cambridge, MA, 1:200) in 2% BSA-PBS overnight at 4 °C, followed by incubation with fluorescently labeled secondary antibodies (Alexa 488-conjugated, Molecular Probes, and TRITC-conjugated, Sigma), for 1 h at 37 °C. All cell experiments were repeated at least three times on different days.

2.7. Fluorescence microscopy

NGF-FITC immobilization, cell polarization and axon extension were analyzed using an inverted phase contrast and fluorescence microscope. Images from the microscope were acquired using a color CCD video camera (Optronics MagnaFire, model S60800) and analyzed using Adobe Photoshop and Image J (NIH). For NGF coating analysis, fluorescence images of NGF-FITC-coated PDMS were captured with a constant exposure time and analyzed for intensity with the imaging software. For the different surface concentrations, experiments were repeated at least four separate times, and a total of 10–20 images were analyzed for fluorescence intensity per condition. Average of fluorescence intensity and standard error of the mean (SEM) are reported, and the average was compared to a calibration curve (see NGF-FITC conjugation section) to determine the surface concentration.

2.8. Polarization and axon length analysis

Based on published criteria, a hippocampal cell was defined as polarized (stage 3) when one of its neurites was at least twice as long as the other neurites and it stained positively for Tau-1 [50,52,53,55]. The fraction of polarized cells was defined as the ratio of cells with axons to the total number of cells per sample. In the same experiments we also measured axon length and angle, which were defined as the straight-line distance from the tip of the axon to the junction between the cell body and axon base, and the angle between this line and a 0° line in the direction of the microchannels (see inset in Fig. 7A). In the case of branched axons, the length of the longest branch was measured from the tip of the axon to the cell body, and then each branch was measured from the tip of the axon to the branch point. All experiments were performed in duplicate at least three times on different days, and an average of 130 cells were analyzed per sample for each condition. P values for fraction of polarized cells and axon length data were analyzed using 2-sided Student's t-test with respect to controls as stated in Tables 1–4. Statistical significance was determined for $P < 0.05$.

2.9. Scanning electron microscopy (SEM)

Microchannels and cells on PDMS were analyzed with a LEO 1530 scanning electron microscope. To image microchannels, patterned PDMS substrates were coated with a gold layer a few angstroms thick and imaged with a typical acceleration voltage of 10 kV. To image neurons, cells on PDMS substrates were fixed with 4% paraformaldehyde (Aldrich) and 4% sucrose in PBS for 20 min, and dehydrated with increasing concentrations of ethanol (30–100%) for a total time of 2 h, followed by 5 min exposure to hexamethyl-disilazane (Sigma). After drying, samples were coated with a gold layer for SEM measurement and imaged with a typical acceleration voltage of 1 kV.

2.10. Atomic force microscopy (AFM)

A Digital Instruments Dimension 3100 with Nanoscope IV controller was used in tapping mode to scan the PDMS substrates and to measure microchannel depth.

3. Results and discussion

3.1. Fabrication of microchannels

Microchannels 1 and 2 μm wide and 400 and 800 nm deep were fabricated using conventional microlithographic techniques. These features were designed and etched on

Table 1
Fraction of polarized cells cultured on substrates with single cues

Substrate properties	Fraction of polarized cells[a]	*P* value (PAA-azido)[b]
PAA-azido (negative control)	0.22 ± 0.02	
Microchannels		
2 μm(W), 400 nm(D)[c]	0.37 ± 0.05	0.0042*
1 μm(W), 400 nm(D)	0.31 ± 0.06	0.0802
2 μm(W), 800 nm(D)	0.39 ± 0.09	0.0158*
1 μm(W), 800 nm(D)	0.32 ± 0.03	0.0274*
Immobilized NGF		
imm. NGF (1 μg)	0.25 ± 0.01	0.1846
imm. NGF (2 μg)	0.28 ± 0.02	0.0440*
Ligand controls		
PAA-azido + sol. NGF (10 ng/mL)	0.24 ± 0.03	0.6128
PAA-azido + sol. NGF (50 ng/mL)	0.31 ± 0.03	0.0348*
Laminin (10 g/mL)	0.29 ± 0.01	0.0400*

*Statistical difference for $\alpha = 0.05$.
[a]Average fraction ± SEM after 20 h in culture for $\langle n \rangle = 5$ (n = number of experimental samples).
[b]2-sided t-test compared to PAA-azido.
[c]W = width; D = depth.

Table 3
Axon lengths for cells cultured on substrates with single cues

Substrate properties	Average length (μm)[a]	*P* value (PAA-azido)[b]
PAA-azido (control)	61.01 ± 1.69	
Microchannels		
2 μm(W), 400 nm(D)	57.16 ± 3.87	0.3188
1 μm(W), 400 nm(D)	64.51 ± 3.63	0.3906
2 μm(W), 800 nm(D)	63.62 ± 3.65	0.4876
1 μm(W), 800 nm(D)	73.01 ± 3.73	0.0012*
Immobilized NGF		
imm. NGF (1 μg)	68.05 ± 1.49	0.0018*
imm. NGF (2 μg)	65.77 ± 1.19	0.0258*
Ligand controls		
PAA-azido + sol. NGF (10 ng/mL)	61.23 ± 2.86	0.9522
PAA-azido + sol. NGF (50 ng/mL)	68.77 ± 2.61	0.0118*
Laminin (10 g/mL)	73.74 ± 2.79	7.64×10^{-5}*

*Statistical difference for $\alpha = 0.05$.
[a]Average length ± SEM after 20 h in culture for $\langle n \rangle = 139$ (n = number of analyzed axons).
[b]2-sided t-test compared to PAA-azido.

Table 2
Fraction of polarized cells cultured on substrates with combinatorial cues

Substrate properties	Fraction of polarized cells[a]	*P* value (PAA-azido)[b]	*P* value (microchannels)[c]	*P* value (NGF)[d]
400-nm *Microchannels*				
2 μm(W), 400 nm(D) + imm. NGF (1 μg)	0.32 ± 0.02	0.0160*	0.3810	0.0284*
1 μm(W), 400 nm(D) + imm. NGF (1 μg)	0.32 ± 0.03	0.0202*	0.7952	0.0388*
2 μm(W), 400 nm(D) + imm. NGF (2 μg)	0.38 ± 0.02	0.0002*	0.8572	0.0060*
1 μm(W), 400 nm(D) + imm. NGF (2 μg)	0.31 ± 0.02	0.0132*	0.9730	0.4224
800-nm *Microchannels*				
2 μm(W), 800 nm(D) + imm. NGF (1 μg)	0.37 ± 0.03	0.0016*	0.8324	0.0020*
1 μm(W), 800 nm(D) + imm. NGF (1 μg)	0.35 ± 0.03	0.0042*	0.5386	0.0072*
2 μm(W), 800 nm(D) + imm. NGF (2 μg)	0.39 ± 0.02	6.5×10^{-5}*	0.9512	0.0026*
1 μm(W), 800 nm(D) + imm. NGF (2 μg)	0.35 ± 0.02	0.0004*	0.3590	0.0240*
Microchannels+soluble NGF				
2 μm(W), 400 nm(D) + sol. NGF (50 ng/mL)	0.30 ± 0.09	0.1754	0.5080	0.9484

*Statistical difference for $\alpha = 0.05$.
[a]Average fraction ± SEM after 20 h in culture for $\langle n \rangle = 5$ (n = number of experimental samples).
[b]2-sided t-test compared to PAA-azido.
[c]2-sided t-test compared to the corresponding microchannel dimensions in the combination.
[d]2-sided t-test compared to the corresponding NGF concentration in the combination.

Table 4
Axon length of cells cultured on substrates with combinatorial cues

Substrate properties	Average length (μm)[a]	*P* value (PAA-azido)[b]	*P* value (microchannels)[c]	*P* value (NGF)[d]
400-nm *Microchannels*				
2 μm(W), 400 nm(D) + imm. NGF (1 μg)	74.16 ± 3.12	0.0002*	0.0006*	0.0680
1 μm(W), 400 nm(D) + imm. NGF (1 μg)	70.83 ± 3.69	0.0084*	0.2396	0.4288
2 μm(W), 400 nm(D) + imm. NGF (2 μg)	68.13 ± 3.47	0.0396*	0.0416*	0.4600
1 μm(W), 400 nm(D) + imm. NGF (2 μg)	76.17 ± 3.30	7.58×10^{-6}*	0.0356*	0.0006*
800-nm *Microchannels*				
2 μm(W), 800 nm(D) + imm. NGF (1 μg)	74.67 ± 4.40	0.0008*	0.0538	0.0826
1 μm(W), 800 nm(D) + imm. NGF (1 μg)	70.93 ± 3.43	0.0074*	0.6832	0.4114
2 μm(W), 0.8 μm(D) + imm. NGF (2 μg)	78.32 ± 3.09	1.38×10^{-7}*	0.0048*	1.02×10^{-5}*
1 μm(W), 0.8 μm(D) + imm. NGF (2 μg)	68.81 ± 2.17	0.0044*	0.3062	0.2248
Microchannels+soluble NGF				
2 μm(W), 400 nm(D) + sol. NGF (50 ng/mL)	74.85 ± 6.63	0.0037*	0.0214*	0.3156

*Statistical difference for $\alpha = 0.05$.
[a]Average length ± SEM after 20 h in culture for $\langle n \rangle = 139$ (n = number of analyzed axons).
[b]2-sided *t*-test compared to PAA-azido.
[c]2-sided *t*-test compared to the corresponding microchannel dimensions in the combination.
[d]2-sided *t*-test compared to the corresponding NGF concentration in the combination.

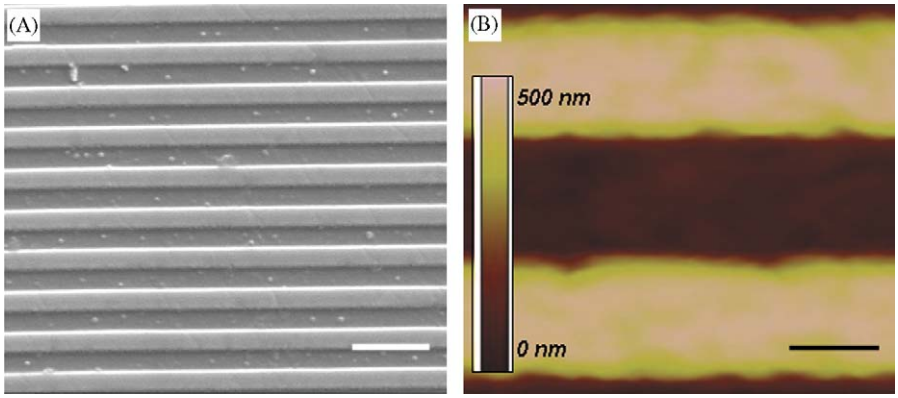

Fig. 2. Microchannel characterization. (A) SEM image of 2 μm-wide and 400 nm-deep channels; (B) AFM image of 2 μm-wide and 400 nm-deep channels. Inset: height color scale. Scale bar = 5 μm (A), 2 μm (B).

silicon wafers that served as masters for the replica molding of PDMS. Fig. 2 illustrates representative SEM and AFM images for the 2 μm-wide and 400 nm-deep channels. Channel depths were also obtained for all other dimensions.

3.2. Immobilization of NGF

Photochemistry methods were utilized for tethering NGF to the surface of PDMS via a photosensitive intermediate layer composed of a backbone of polyallylamine with several pending phenylazido functional groups (PAA-azido) (Fig. 1). This cross-linking compound was obtained from the acylation of PAA by the reaction of amine groups from the polymer with *N*-4-(azidobenzoyloxy)succinimide, which incorporated the phenylazido moiety. UV-Vis spectra were used to confirm the effective incorporation of the photosensitive group by measuring absorbance of the conjugate at 280 nm (results not shown). The final PAA-azido conjugate served as an intermediate linker for immobilizing NGF by activation of the phenylazido compounds with UV light and the subsequent non-specific insertion into different bonds.

To analyze and detect the effectiveness of the immobilization, NGF was labeled with FITC, which was only used for detection purposes and not for cell culture. As observed in Fig. 3, the chosen photochemistry permitted the immobilization of the protein in different schemes. In Figs. 3A and B, NGF-FITC was homogeneously immobilized using a UV lamp, either on plain PDMS or over and within microchannels. This was the procedure used for all other experiments in this investigation. However, we also explored two more immobilization variations to show the versatility of the procedure. As shown in Figs. 3C and D, the growth factor could also be selectively patterned using either a mask during the exposure step with the UV lamp or using a precisely focused UV laser (Nd:YAG laser at 355 nm). A pattern from a TEM grid was successfully

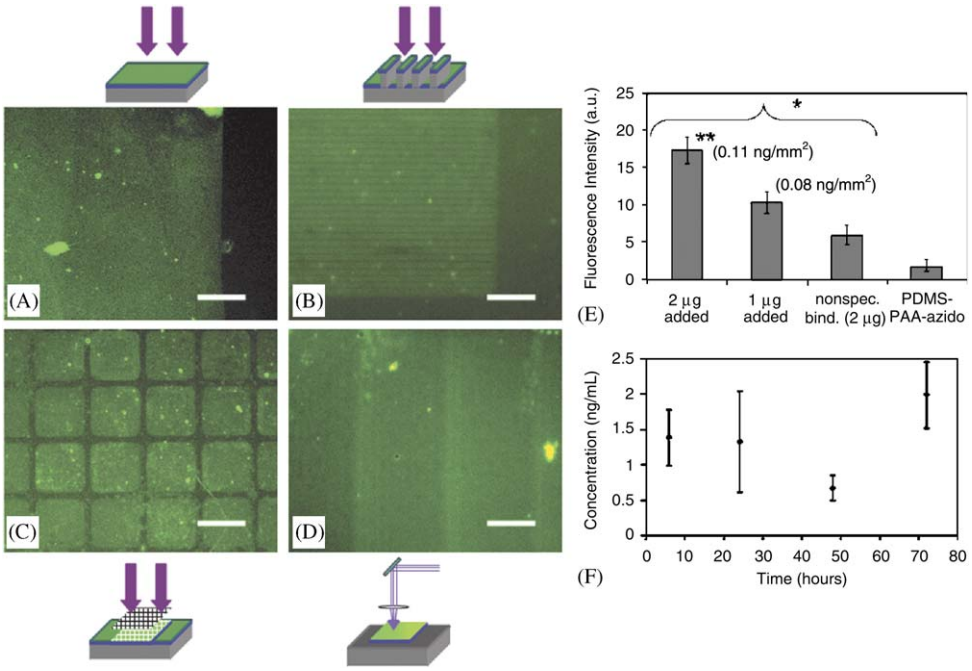

Fig. 3. Fluorescence images of immobilized NGF-FITC on PDMS. (A) Interface between NGF-FITC-immobilized and no-NGF areas; (B) interface between 2 μm channels with immobilized NGF-FITC and smooth PDMS with immobilized NGF-FITC; (C) TEM grid pattern of immobilized NGF-FITC transferred to PDMS by exposure with UV lamp; (D) NGF-FITC gradient immobilization with Nd:YAG laser (three consecutive gradients) by changing the scanning rate for each 20 μm line from 20 to 180 μm/s; (E) quantitative analysis of fluorescence intensity ± SEM for samples with different surface concentrations and controls (*X*-axis: total protein added before immobilization). The values in parenthesis correspond to the approximate surface concentrations determined by comparing the average of the fluorescence intensity with a previously obtained calibration curve; (F) ELISA analysis of concentration of soluble NGF released from PDMS surfaces over time ($n = 3$). Error bars correspond to SEM. * Statistically significant differences from PDMS-PAA-azido using *t*-test with $P < 0.05$. ** Statistically significant difference from non-specific binding control using *t*-test with $P < 0.00001$. Scale bars = 30 μm (A and B), 100 μm (C and D).

transferred to the surface of the PDMS using a UV lamp (Fig. 3C), and a laser was used to create gradients by modulating the scanning rate of the laser (Fig. 3D). These results successfully established the presence of the tethered protein on the surface of the material, which also indirectly confirmed the activation of the phenyl-azido groups with UV light, as NGF was only immobilized in the irradiated areas to create patterns.

NGF-FITC was also used to obtain an estimate of the surface concentration of the protein on PDMS. For this analysis, fluorescence intensity of the samples was compared with a calibration curve obtained by casting known quantities of NGF-FITC on defined areas. For the fluorescence intensity shown in Fig. 3E, the approximate surface concentrations obtained when 1 or 2 μg of NGF were initially added corresponded to 0.08 and 0.11 ng/mm^2, respectively. These values correspond to roughly a 10% surface coverage when compared to the concentration of a typical protein monolayer (1 ng/mm^2) [70]. These values are similar to previous publications on immobilized NGF with concentrations of about 25 ng/cm^2 [36]. However, it is important to clarify that probably not all immobilized NGF was biologically active, and the exact percentage of active protein is challenging to analyze.

Although we demonstrated the presence of the immobilized growth factor on the surface of PDMS, we also observed non-specific binding of NGF (without reaction) as illustrated in Fig. 3E. The possible release into the media of this adsorbed NGF was analyzed with a time-course ELISA assay. This was important to consider to ensure that the observed effects on cells were caused by the immobilized and not the soluble form of NGF. Sample volumes were collected from PDMS-NGF substrates incubated in PBS at 37 °C for 72 h (Fig. 3F). The average concentration of NGF in solution was 1.34 ± 0.44 ng/mL ($n = 3$) which has negligible cellular effects [57]. Although soluble and immobilized concentrations cannot be directly compared, the soluble NGF concentration was probably much smaller than the immobilized NGF concentration (0.001 ng/mm^3 compared to 0.11 ng/mm^2).

3.3. Polarization of hippocampal cells on microchannels and immobilized NGF

Embryonic hippocampal cells in culture have been extensively studied because of their ability to spontaneously establish a single axon from equally growing neurites. These cells are the ideal model for analyzing axon initiation mechanisms, which involve accumulation of different markers in the neurite that becomes the axon [52–55]. We investigated how these cells polarized on a material with different surface properties such as

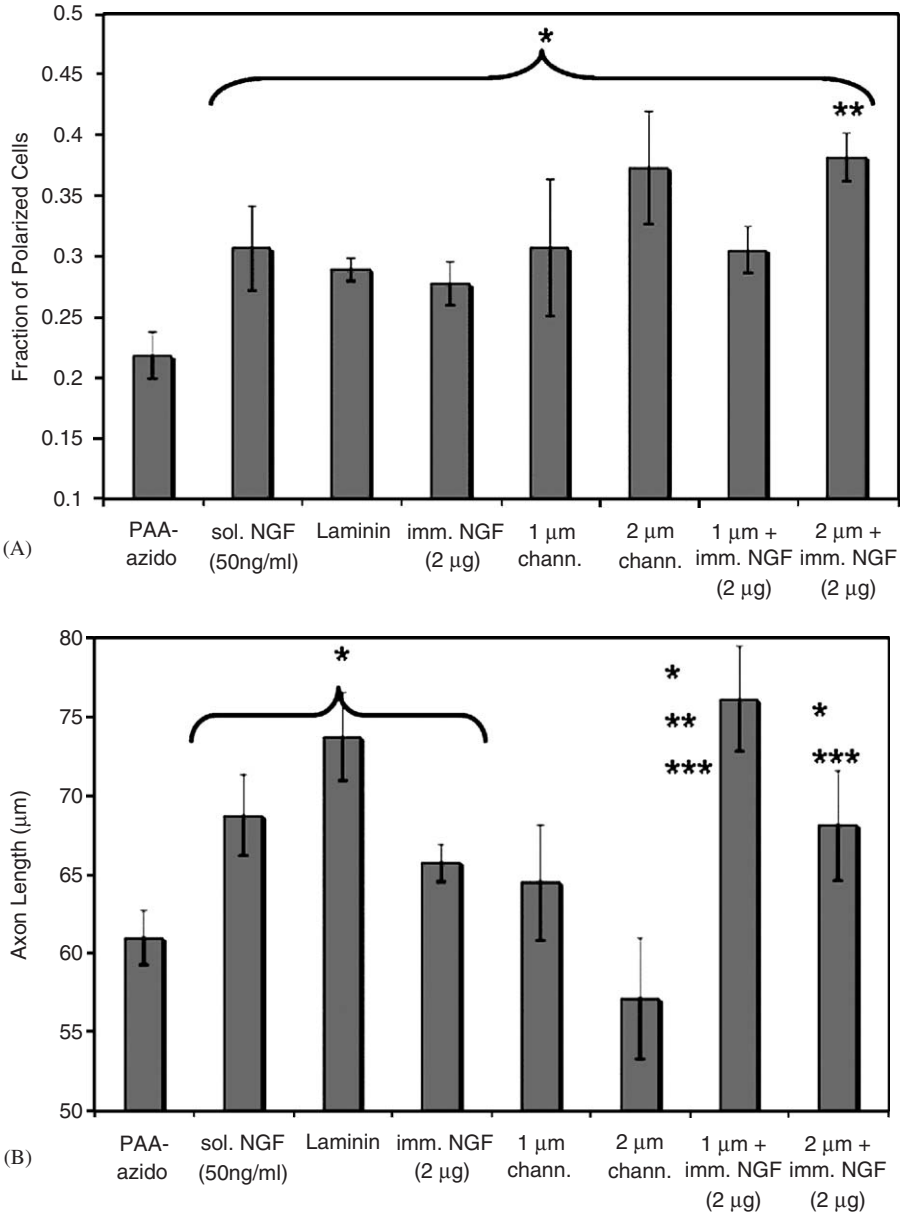

Fig. 4. Contrasting effects of microchannels versus immobilized NGF on polarization and axon length. Representative data (complete data in Tables 1–4) of polarization and axon length of hippocampal cells cultured for 20 h on PDMS with different surface properties. (A) Fraction of polarized hippocampal cells cultured on PDMS with different physical and chemical surface properties as stated in the *X*-axis. There was no additive effect from the combination of immobilized NGF and topography. *, ** Statistically significant differences from PDMS-PAA-azido and immobilized NGF alone, respectively, using *t*-test with $P < 0.05$; (B) axon length of hippocampal cells cultured on PDMS with different physical and chemical surface properties as stated in the *X*-axis. There was a synergistic effect from the combination of immobilized NGF and topography. *, **, *** Statistically significant differences from PDMS-PAA-azido, microchannels alone and immobilized NGF alone, respectively, using *t*-test with $P < 0.05$.

topography provided by microchannels or bioactivity mediated by an active ligand. As observed in Tables 1 and 2 and Figs. 4 and 5, there was a defined effect on the fraction of stage 3 cells after 20 h in culture, depending on the surface characteristics.

Table 1 summarizes the results for individual stimuli presented on the surface of PDMS, which included physical cues (microchannels of 400 and 800 nm depth and 1 and 2 μm width) and biochemical cues (immobilized NGF or adsorbed laminin). These data suggest that the greatest effect for a single stimulus on the percentage of polarized cells was obtained by the presence of microchannels, more specifically of 2 μm width, in which there was an increase of 68–72% in the number of cells with an established axon compared to smooth substrates (i.e., PAA-azido only). The substrates with immobilized NGF also accelerated neuron polarization but to a lesser extent, with a 27% increase in stage 3 cells with respect to PAA-azido-only substrates. Although this effect was less pronounced than for topography, it was statistically higher than PAA-azido

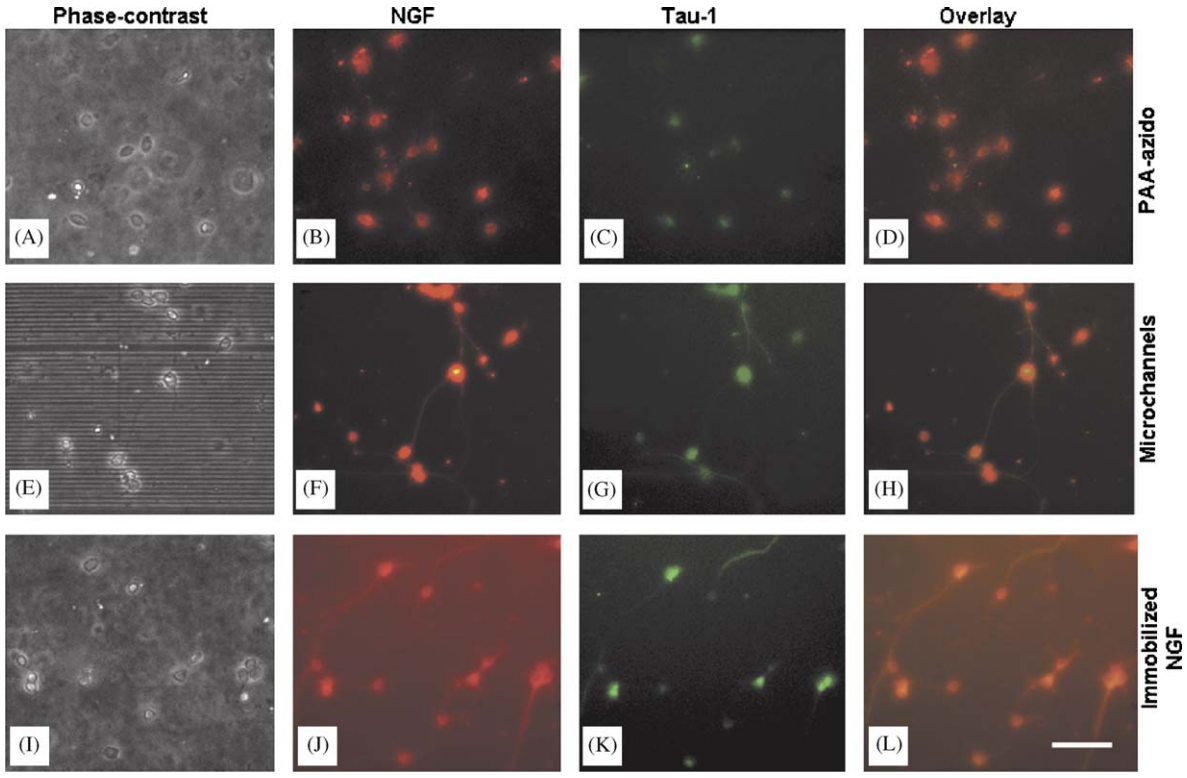

Fig. 5. Phase-contrast and fluorescence photomicrographs of hippocampal cells on PDMS with individual stimuli. (A–D) Cells cultured on PDMS-PAA-azido only; (E–H) cells cultured on 2 μm-wide and 400 nm-deep microchannels; (I–L) cells cultured on immobilized NGF (0.11 ng/mm^2). Green (Alexa 488) and red (TRITC) labeling correspond to Tau-1 and NGF, respectively. Immobilized NGF on the surface was detected from substrate fluorescence, as shown in images (J–L). Scale bar = 50 μm.

controls ($P = 0.04$), and statistically indistinguishable from controls with either soluble NGF (50 ng/mL) ($P = 0.46$) or laminin coating (10 μg/mL) ($P = 0.74$).

It is important to emphasize that these cellular responses were not the result of soluble NGF that had leached out from the surface; only 1 ng/mL of NGF was detected with ELISA assays and controls with 10 ng/mL soluble NGF did not elicit any significant polarization of hippocampal cells (see Table 1). In addition, it is also important to clarify that although hippocampal cells have intracellular NGF compartments, as seen from the NGF labeling in Figs. 5 and 6, these cells only release NGF in very low quantities (~4–8 pg/mL for transfected cells with increased NGF expression) and as a consequence of high levels of calcium or glutamate for example [60].

Physical and biochemical stimuli were combined in a single modified material surface to investigate if the combination of these two simultaneous cues could further enhance axon initiation. In this case, microchannels were coated with immobilized NGF (as in Fig. 3B) and cells observed for polarization. As summarized in Table 2 and Fig. 4A, the combination strategy with 1 and 2 μm channels (400 nm deep) and immobilized NGF (both with 1 and 2 μg added) was statistically different from immobilized NGF only, but not statistically different from topography only, suggesting that contact guidance was the dominant stimulus. Similar behavior was observed with 800 nm-deep microchannels. The same result was also obtained when the cells were incubated on microchannels and NGF in solution. *This suggests that although both soluble and immobilized NGF did increase the rate of polarization and the establishment of a single axon, these effects were attenuated in the presence of surface topography, which appears to be a dominant signal for polarization.*

The effects of NGF in hippocampal cells have been controversial, as NGF seems to produce both an increase in the rate of polarization and apoptosis [57,61,62]. Nevertheless, Brann et al. [62] proposed that such varied responses are correlated to neuron age. This age effect is related to NGF intracellular pathway through ceramide derived from sphingomyelin hydrolysis after binding to $p75^{NTR}$ receptor, as these cells do not express the high-affinity TrKA receptors. Although increased intracellular levels of ceramide do increase the number of cells in stage 3 during the first 24 h in culture, these ceramide levels also get much higher as the expression of $p75^{NTR}$ receptor increases with time and the production of ceramide increases accordingly, which ultimately ends in apoptosis.

With regard to enhanced neuron polarization, previous studies have demonstrated beneficial effects of soluble NGF with concentrations between 50 and 200 ng/mL in cultures with and without a supporting layer of glia [57]. An approximate increase of 32% in stage 3 neurons with 50–100 ng/mL of soluble NGF without glia has been

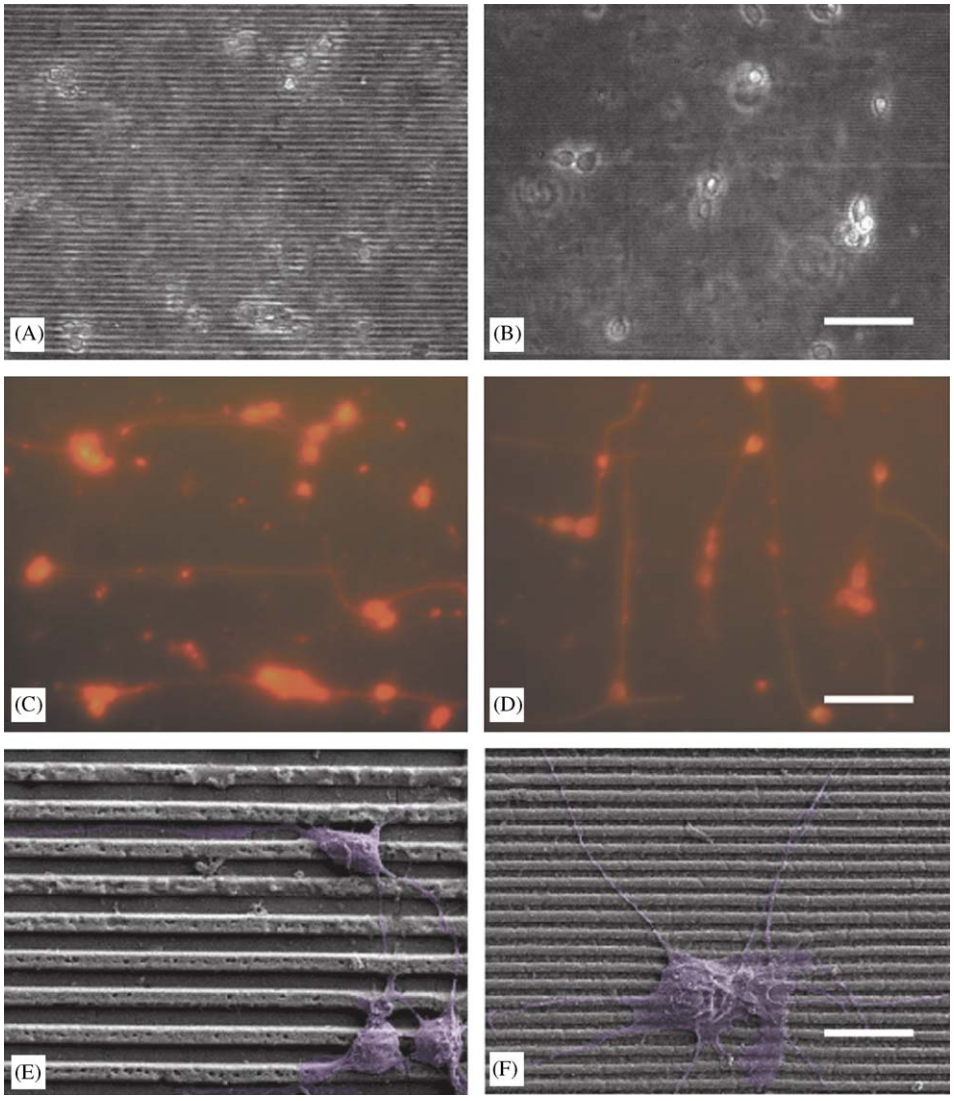

Fig. 6. SEM, phase-contrast and fluorescence photomicrographs of hippocampal cells on PDMS with combinatorial stimuli. (A, C, E) Cells cultured on 2 μm-wide and 800 nm-deep microchannels with immobilized NGF (0.11 ng/mm^2); (B, D, F) cells cultured on 1 μm-wide and 400 nm-deep microchannels with immobilized NGF (0.11 ng/mm^2). Fluorescence images correspond to the overlay of Tau-1 (green, Alexa 488) and NGF (red, TRITC) labeling. Neurons extended longer and more oriented axons on surfaces with combinatorial cues. Scale bars = 50 μm (A–D), 10 μm (E and F).

reported, which was analogous to the 36% increase observed in our control experiments with 50 ng/mL of NGF. Our results also suggest that these effects are similar when the growth factor is presented in an immobilized form with an approximate surface concentration of 0.1 ng/mm^2 (see Table 1). Although p75^{NTR} receptor produces clathrin-coated vesicles after NGF binding, this occurs at a much slower rate than for TrkA receptors [63], which suggests that intracellular cascades could be triggered at the cellular membrane, an advantage for applications with material-bound ligands. More importantly, signaling from this receptor does not require endocytosis as sphingomyelin hydrolysis (ceramide source) is not reduced when internalization is prevented [64]. This evidence supports the fact that immobilized NGF could have an effect on hippocampal cells similar to soluble NGF. Although tethered ligands cannot be internalized, the binding of immobilized NGF to P75^{NTR} receptor could be sufficient to trigger ceramide production and therefore, accelerate polarization.

The effects of surface topography in polarization have been investigated to a lesser extent. Dowell-Mesfin et al. showed that pillars of 2 μm width increased the number of cells in stage 3 after 24 h in culture [59], but quantitative measurements and comparison with chemical ligands have not been performed. More recently, Foley et al. [68] showed increased neuritogenesis on nano-ridges in PC12 cells with low levels of NGF, and Ahmed et al. [9] reported an increase in neurite generation in several neuronal types cultured on nanofibers. We confirmed that microtopography increases the number of cells in stage 3 after 20 h in culture, with a 68% and 72% increase for 2 μm microchannels (400 and 800 nm, respectively) and a 36% and 42% increase for 1 μm microchannels (400 and 800 nm, respectively) with respect to PAA-azido-only (smooth)

substrates (Table 1). Furthermore, our results suggest that the effect of topography on the rate of polarization was greater than other controls such as NGF in solution or laminin.

Intracellular signaling derived from contact guidance cues is less well understood than growth factor signaling. These responses are thought to be transduced by tension generated within the cytoskeleton and the redistribution of focal adhesion complexes (FAC) caused by surface topography (reviewed in [65]). In particular, integrins in FAC are important modulators of intracellular signaling, and additionally, the cytoskeleton is directly connected to the nuclear membrane, which ultimately alters morphology of the nucleus in the presence of topography. It has been hypothesized that nuclear alignment could be connected to changes in gene expression [65]; for example it was shown by Dalby et al. [66] that numerous genes were upregulated in fibroblasts when nuclei were aligned as a consequence of surface topography. Based on this, polarization in hippocampal cells could be highly influenced by topographical features as a consequence of signal transduction by the cytoskeleton to the nucleus, and subsequent effects on protein translation. We speculate, given the results from the present studies, that signal transduction through the cytoskeleton could be more effective in triggering polarization compared to signaling from NGF.

3.4. Axon length and orientation of hippocampal cells

In addition to analyzing the fraction of stage 3 cells, we also analyzed the length and orientation of the already established axons, and, interestingly, the results were not analogous. Immobilized NGF alone elicited an increase of 10% in axon length with respect to PAA-azido only samples, whereas topography did not significantly affect axon length, except for microchannels of 1 μm width and 800 nm depth, which had an increase of 20% (Table 3). Although we expected an increase in axon initiation to be correlated with longer axons, the results revealed that topography had little effect on elongation rate after polarization. In contrast, neurons exposed to immobilized NGF had initially slower polarization, but the growth rate must have been enhanced after initiation to ultimately produce longer axons. NGF in solution (50 ng/mL) and laminin also appeared to have more pronounced effects on axon length than on axon initiation, as these ligands produced an increase in length of 10% and 20%, respectively, compared with PAA-azido-only substrates. Again, the similarity in responses between immobilized NGF and soluble NGF, exhibiting the same increase in length, further supports the possibility of triggering equivalent intracellular cascades.

Quantitative analysis of the effects of soluble NGF on axon length in hippocampal cells has not been reported before. However, Schwarz and Futerman [67] investigated the effect of adding ceramide stereoisomers to hippocampal cell cultures, which would mimic the effect of NGF, as ceramide is critical in the intracellular pathway of NGF as discussed before. In that study, an increase of 40% in length was detected with large quantities of ceramide (5 μM), although this cannot be directly correlated to a particular amount of NGF. However, the authors reported that a significant increase in the number of polarized cells was achievable with much lower concentrations of ceramide (0.05–0.1 μM), which suggested that low concentrations of ceramide might be effective in enhancing polarization, but not axon growth extensively. In other words, ceramide produced from NGF binding to $p75^{NTR}$ would more effectively impact polarization than axon elongation, although the overall effect on polarization is small when compared to topography, and the effect on growth is significant when compared to topography as well. Here we observed a rather small increase of 10% in length for both soluble and immobilized forms of NGF, although the difference was statistically different from controls with PAA-azido-only substrates ($P<0.03$).

In addition to polarization, we were interested in combining microchannels and immobilized NGF to detect any cooperative enhancement in axon length. As observed in Table 4, there seemed to be an effect from the combination of stimuli as surfaces with both cues had a maximum increase of 21% and 25% in length for 2 and 1 μm microchannels (400 nm depth), respectively, compared with PAA-azido-only samples. These percentages were significantly different from the values for individual stimuli (see P values in Table 4), and because topography alone did not elicit an increase in neurite length, a synergy mechanism must have been present. There was a similar trend for 800 nm-deep and 2 μm-width microchannels, with an increase of 28% in length compared to PAA-azido, but there was not a significant combinatorial effect for the 1 μm channels, which already had a large effect when the topography was presented individually (20%). The observed synergy might be a product of faster polarization on topography in conjunction with the enhanced growth rate from NGF, which might ultimately yield longer axons. This suggests that to have the longest neurites, it is necessary to combine fast initiation with fast growth, which in this study was obtained by combining topographical plus bioactive properties on the material surface.

In relation to axon orientation, we observed results similar to those published for hippocampal cells in the literature [18,69] (Figs. 6 and 7). Figs. 6 and 7A illustrate that cells tended to grow perpendicular (angle = 90°) to the 1 μm microchannels (400 nm deep), and to some extent also in the 2 μm channels, although for this width cells also grew in a parallel fashion (angle = 0° or 180°). However, as depth increased to 800 nm the percentage of cells growing parallel to the microchannels increased, which was more dramatically observed for the 2 μm channels (Figs. 6 and 7B).

Effects of topography on neurite length and orientation have been reported previously. Rajnicek et al. demonstrated that smaller widths produce longer neurites [18],

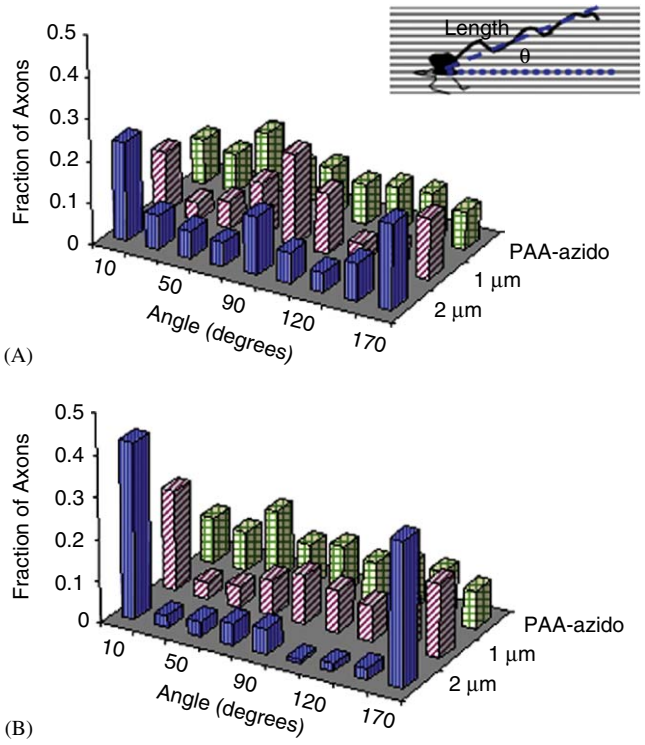

Fig. 7. Axon orientation of hippocampal cells after 20 h in culture on PDMS with different surface properties. (A) Angle distribution for axons growing on 400 nm-deep microchannels with 0.11 ng/mm^2 of immobilized NGF ($n = 287$, 137, 122, for PAA-azido, 1 and 2 μm, respectively). Inset: schematic illustrating how axon length and angle were analyzed; (B) angle distribution for axons growing on 800 nm-deep microchannels with 0.11 ng/mm^2 of immobilized NGF ($n = 287$, 198, 170, for PAA-azido, 1 and 2 μm, respectively). Axons tended to grow parallel to microchannels as depth and width increased.

which is also suggested in Table 3, although we only saw significant differences from the control for the 1 μm-wide and 800 nm-deep channels. Perpendicular and parallel growth to microchannels was also thoroughly investigated by the same group, showing parallel orientation for increasing widths and depths, and demonstrating the important role of calcium influx and protein kinase C in this behavior [69]. More recently, Dowell-Mesfin et al. [59] reported that after 14 days of culture, hippocampal cells had longer neurites for smaller distances between ridges and neurites tended to bridge between adjacent pillars, which can also be observed in Fig. 6F. This bridging is what finally allows the neurites to grow in a perpendicular fashion, which becomes more difficult as groove width increases. These authors also reported changes in growth cone morphology depending on the gap size between pillars, with growth cones having more "narrow profiles" for the smaller gaps. Based on this observation, we speculate that 1 μm-wide and 800 nm-deep microchannels could have the largest effect on neurite length because the growth cone is more restricted in movement and morphology. Similarly, the impact of smaller patterns on axon length could have also played a role in the synergy observed for 1 μm microchannels (400 depth) and immobilized NGF.

4. Conclusions

We have investigated hippocampal cell responses to different material surface properties, including microtopography and immobilized NGF. We found that immobilized NGF (0.1 ng/mm^2) produced similar responses as soluble NGF (50 ng/mL), which allowed us to hypothesize the equivalence of intracellular pathways, even without endocytosis in the immobilized form. Neuron polarization was analyzed and we found that surface topography influenced more effectively the fraction of stage 3 neurons (68% compared to controls) than biochemical ligands such as NGF or laminin (30% increase). Furthermore, when both types of cues were simultaneously presented on the surface of PDMS (i.e., microchannels plus tethered NGF) there was only a significant increase with respect to immobilized NGF but not to topography itself, suggesting that physical signals have a dominant effect on polarization mechanisms.

In contrast, effects on axon length seemed to be opposite. Immobilized NGF had a greater but modest increase (10% increase with respect to controls), whereas topography did not have a significant effect (except for 1 μm-width and 800 nm-depth). However, a synergistic enhancement was observed when both contact guidance and growth factor were presented simultaneously on the surface (25% increase), which could be a result of faster polarization from topography plus increased growth rate from NGF. Finally, axon orientation was also investigated. Our data were consistent with previous results, with more parallel alignment of axons with larger widths and depths for microchannels.

These studies not only compared responses between chemical and physical stimuli, but also investigated how these cues are modulated when presented simultaneously on the surface of a material. *Axon formation* (*initiation*) *and axon growth* (*maintenance*) *were independently studied, and our results suggest a more prominent effect of topography on initiation, in contrast to the more effective role of immobilized NGF in axon growth after initiation.* These data imply the need to combine fast initiation with fast growth to ultimately achieve longer axons, which was accomplished here by combining biochemical and physical properties on the surface of the material. From this it is evident that surface characteristics can be precisely engineered to present combinatorial cues that target multiple cellular transduction mechanisms to finally produce enhanced neuronal responses. These results can be potentially applied to the design of biomaterials used to interface with neurons.

Acknowledgments

Funding for this work was provided by a grant from the Gillson Longenbaugh Foundation to C.E.S., and partial support from the US National Science Foundation and the Office of Naval Research to S.C.C. We thank the Welch

Foundation and SPRING for partial financial support in the CNM facilities.

References

[1] Shin H, Jo S, Mikos AG. Biomimetic materials for tissue engineering. Biomaterials 2003;24(24):4353–64.

[2] Drotleff S, Lungwitz U, Breunig M, Dennis A, Blunk T, Tessmar J, et al. Biomimetic polymers in pharmaceutical and biomedical sciences. Eur J Pharm Biopharm 2004;58(2):385–407.

[3] Kasemo B. Biological surface science. Surf Sci 2002;500(1–3):656–77.

[4] Ito Y. Tissue engineering by immobilized growth factors. Mater Sci Eng C 1998;6:267–74.

[5] Simmons CA, Alsberg E, Hsiong S, Kim WJ, Mooney DJ. Dual growth factor delivery and controlled scaffold degradation enhance in vivo bone formation by transplanted bone marrow stromal cells. Bone 2004;35(2):562–9.

[6] Kent Leach J, Kaigler D, Wang Z, Krebsbach PH, Mooney DJ. Coating of VEGF-releasing scaffolds with bioactive glass for angiogenesis and bone regeneration. Biomaterials 2006;27:3749–55.

[7] Miller C, Jeftinija S, Mallapragada S. Micropatterned Schwann cell-seeded biodegradable polymer substrates significantly enhance neurite alignment and outgrowth. Tissue Eng 2001;7:705–15.

[8] Miller C, Jeftinija S, Mallapragada S. Synergistic effects of physical and chemical guidance cues on neurite alignment and outgrowth on biodegradable polymer substrates. Tissue Eng 2002;8:367–78.

[9] Ahmed L, Liu H, Mamiya P, Ponery AS, Babu AN, Weik T, et al. Three-dimensional nanofibrillar surfaces covalently modified with tenascin-C-derived peptides enhance neuronal growth in vitro. J Biomed Mater Res Part A 2006;76A(4):851–60.

[10] Sirois E, Cote MF, Doillon CJ. Growth factors and biological supports for endothelial cell lining: in vitro study. Int J Artif Organs 1993;16(8):609–19.

[11] Harrison RG. Experiments in transplanting limbs and their bearing upon the problems of the development of nerves. J Exp Zool 1907;4:239–81.

[12] Goslin K, Banker G. Experimental observations on the development of polarity by hippocampal neurons in culture. J Cell Biol 1989;108:1507–16.

[13] Zhang N, Yan H, Wen X. Tissue-engineering approaches for axonal guidance. Brain Res Rev 2005;49(1):48–64.

[14] Schmidt CE, Leach JB. Neural tissue engineering: strategies for repair and regeneration. Annu Rev Biom Eng 2003;5:293–347.

[15] Clark P, Britland S, Connolly P. Growth cone guidance and neuron morphology on micropatterned laminin surfaces. J Cell Sci 1993;105:203–12.

[16] Saneinejad S, Shoichet MS. Patterned glass surfaces direct cell adhesion and process outgrowth of primary neurons of the central nervous system. J Biomed Mater Res 1998;42:13–9.

[17] Zhang Z, Yoo R, Wells M, Beebe Jr TP, Biran R, Tresco P. Neurite outgrowth on well-characterized surfaces: preparation and characterization of chemically and spatially controlled fibronectin and RGD substrates with good bioactivity. Biomaterials 2005;26(1):47–61.

[18] Rajnicek A, Britland S, McCaig C. Contact guidance of CNS neurites on grooved quartz, influence of groove dimensions, neuronal age and cell type. J Cell Sci 1997;110(23):2905–13.

[19] Clark P, Connolly P, Curtis AS, Dow JA, Wilkinson CD. Topographical control of cell behavior. Development 1987;99: 439–48.

[20] Mahoney MJ, Chen RR, Tan J, Saltzman WM. The influence of microchannels on neurite growth and architecture. Biomaterials 2005;26(7):771–8.

[21] Moore K, Macsween M, Shoichet M. Immobilized concentration gradients of neurotrophic factors guide neurite outgrowth of primary neurons in macroporous scaffolds. Tissue Eng 2006;12(2):267–78.

[22] Xu X, Yee W, Hwang P, Yu H, Wan C, Gao S, et al. Peripheral nerve regeneration with sustained release of poly(phosphoester) micro-encapsulated nerve growth factor within nerve guide conduits. Biomaterials 2003;24:2405–12.

[23] Schmidt CE, Shastri VR, Vacanti JP, Langer R. Stimulation of neurite outgrowth using an electrically conducting polymer. Proc Natl Acad Sci USA 1997;94:8948–53.

[24] Norris CR, Kalil K. Guidance of callosal axons by radial glia in the developing cerebral cortex. J Neurosci 1991;11(11):3492–841.

[25] Singer J, Nordlander RH, Egar M. Axonal guidance during embryogenesis and regeneration in the spinal cord of the newt: the blueprint hypothesis of neuronal pathway patterning. J Comp Neurol 1979;185:1–22.

[26] Clark P, Connolly P, Curtis AS, Dow JA, Wilkinson CD. Topographical control of cell behavior, II. multiple grooved substrata. Development 1990;108:635–44.

[27] Curtis A, Wilkinson C. Topographical control of cells. Biomaterials 1997;18:1573–83.

[28] Clark P, Connolly P, Curtis AS, Dow JA, Wilkinson CD. Cell guidance by ultrafine topography in vitro. J Cell Sci 1991;99:73–7.

[29] Curtis A, Wilkinson C, Wojciak-Stothard B. Cell guidance, movement and growth, accelerating cell movement. Cell Eng Inc Mol Eng 1995;1:35–8.

[30] Ebadi M, Bashir RM, Heidrick ML, Hamada FM, El Refaey H, Hamed A, et al. Neurotrophins and their receptors in nerve injury and repair. Neurochem Int 1997;30(4/5):347–74.

[31] Letourneau PC. Chemotactic response of nerve fiber elongation to nerve growth factor. Develop Biol 1978;66:183–96.

[32] Zhang Y, Moheban DB, Conway BR, Bhattacharyya A, Segal RA. Cell surface Trk receptors mediate NGF-induced survival while internalized receptors regulate NGF-induced differentiation. J Neurosci 2000;20(15):5671–8.

[33] Campenot RB. NGF and the local control of nerve terminal growth. J Neurobiol 1994;25(6):599–611.

[34] Aoki K, Nakamura T, Matsuda M. Spatio–temporal regulation of Rac1 and Cdc42 activity during nerve growth factor-induced neurite outgrowth in PC12 cells. J Biol Chem 2004;279(1):713–9.

[35] Ito Y. Regulation of cellular gene expression by artificial materials immobilized with biosignal molecules. Jpn J Artif Organs 1998;27(2):541–4.

[36] Kapur TA, Shoichet MS. Chemically-bound nerve growth factor for neural tissue engineering applications. J Biomater Sci Polym Edn 2003;14(4):383–94.

[37] Kapur TA, Shoichet MS. Immobilized concentration gradients of nerve growth factor guide neurite outgrowth. J Biomed Mater Res 2004;68A:235–43.

[38] Gallo G, Lefcort FB, Letourneau PC. The TrkA receptor mediates growth cone turning toward a localized source of nerve growth factor. J Neurosci 1997;17(14):5445–54.

[39] Gallo G, Letourneau PC. Localized sources of neurotrophins initiate axon collateral sprouting. J Neurosci 1998;18(14):5403–14.

[40] Naka Y, Kitazawa A, Akaishi Y, Shimizu N. Neurite outgrowth of neurons using neurothophin-coated nanoscale magnetic beads. J Biosci Bioeng 2004;98(5):348–52.

[41] Ito Y, Kondo S, Chen G, Imanishi Y. Patterned artificial juxtacrine stimulation on cells by covalently immobilized insulin. FEB Lett 1997;403:159–62.

[42] Chen G, Ito Y, Imanishi Y. Photoimmobilization of epidermal growth factor enhances its mitogenic effect by artificial juxtacrine signaling. Biochim Biophys Acta 1997;1358:200–8.

[43] Zisch AH, Chenk U, Schense JC, Sakiyama-Elbert SE, Hubbel JA. Covalently conjugated VEGF-fibrin matrices for endothelialization. J Controll Release 2001;71:101–13.

[44] Patai S. The chemistry of azido group. London: Interscience Publishers; 1971.

[45] Scriven EF. Azides and nitrenes, reactivity and utility. Orlando: Academic Press; 1984.

[46] Matsuda T, Sugawara T. Photochemical protein fixation on polymer surfaces via derivatized phenyl azido group. Langmuir 1995;11: 2272–6.

[47] Ito Y, Chen G, Imanishi Y. Micropatterned immobilization of epidermal growth factor to regulate cell function. Bioconjugate Chem 1998;9:277–82.
[48] Chen G, Ito Y. Gradient micropattern immobilization of EGF to investigate the effect of artificial juxtacrine stimulation. Biomaterials 2001;22:2453–7.
[49] Chung TW, Lu YF, Wang SS, Lin YS, Chu SH. Growth of human endothelial cells on photochemically grafted Gly–Arg–Asp (GRGD) chitosans. Biomaterials 2002;23:4803–9.
[50] Dotti CG, Sullivan CA, Banker GA. The establishment of polarity by hippocampal neurons in culture. J Neurosci 1988;8(4):1454–68.
[51] Fukata Y, Kimura T, Kaibuchi K. Axon specification in hippocampal cells. Neurosci Res 2002;43:305–15.
[52] Schwamborn JC, Puschel AW. The sequential activity of the GTPases Rap1B and Cdc42 determines neuronal polarity. Nat Neurosci 2004;7:923–9.
[53] Menager C, Arimura N, Fukata Y, Kaibuchi K. PIP_3 is involved in neuronal polarization and axon formation. J Neurochem 2004;89:109–18.
[54] Jiang H, Guo W, Liang X, Rao Y. Both the establishment and the maintenance of neuronal polarity require active mechanisms: critical roles of GSK-3β and its upstream regulator. Cell 2005;120:123–35.
[55] Nishimura T, Hato K, Vamguchi T, Fukata Y, Ohno S, Kaibuchi K. Role of the PAR-3-KIF3 complex in the establishment of neuronal polarity. Nat Cell Biol 2004;6:328–34.
[56] Lein PJ, Banker GA, Higgins D. Laminin selectively enhances axon growth and accelerates the development of polarity by hippocampal neurons in culture. Develop Brain Res 1992;69:191–7.
[57] Brann AB, Scott R, Neuberger Y, Abufalia D, Boldin S, Fainzilber M, et al. Ceramide signaling downstream of the p75 neurotrophin receptor mediates the effects of nerve growth factor on outgrowth of cultured hippocampal neurons. J Neurosci 1999;19(19):8199–206.
[58] Lamoureux P, Ruthel G, Bauxbaum RE, Heidemann SR. Mechanical tension can specify axonal fate in hippocampal cells. J Cell Biol 2002;159:499–508.
[59] Dowell-Mesfin NM, Abdul-Karim M-A, Turner AM, Schanz S, Craighead HG, Roysam B, et al. Topographically modified surfaces affect orientation and growth of hippocampal neurons. J Neural Eng 2004;1:78–90.
[60] Blochl A, Thoenen H. Characterization of nerve growth factor (NGF) release from hippocampal neurons: evidence for a constitutive and an unconventional sodium-dependent regulated pathway. Eur J Neurosci 1995;7:1220–8.
[61] Friedman WJ. Neurotrophins induce death of hippocampal neurons via the p75 receptor. J Neurosci 2000;20(17):6340–6.
[62] Brann AB, Tcherpakov M, Williams IM, Futerman AH, Fainzilber M. Nerve growth factor-induced p75-mediated death of cultured hippocampal neurons is age-dependent and transduced through ceramide generated by neutral sphingomyelinase. J Biol Chem 2002;277(12):9812–8.
[63] Bronfman FC, Tcherpakov M, Jovin TM, Fainzilber M. Ligand-induced internalization of the p75 neurotrophin receptor: a slow route to the signaling endosome. J Neurosci 2003;23(8):3209–20.
[64] Dobrowsky RT, Jenkins GM, Hannun YA. Neurotrophins induce sphingomyelin hydrolysis. J Biol Chem 1995;270(38):22135–42.
[65] Dalby MJ. Topographically induced direct cell mechanotransduction. Med Eng Phys 2005;27(9):730–42.
[66] Dalby MJ, Riehle MO, Yarwood SJ, Wilkinson CDW, Curtis ASG. Nucleus alignment and cell signaling in fibroblasts: response to a micro-grooves topography. Exp Cell Res 2003;284:274–82.
[67] Schwarz A, Futerman AH. Distinct roles for ceramide and glucosylceramide at different stage of neuronal growth. J Neurosci 1997;17(9):2929–38.
[68] Foley JD, Grunwald EW, Nealey PF, Murphy CJ. Cooperative modulation of neuritogenesis by PC12 cells by topography and nerve growth factor. Biomaterials 2005;26(17):3639–44.
[69] Rajnicek AM, McCaig CD. Guidance of CNS growth cones by substratum grooves and ridges: effects of inhibitors of the cytoskeleton, calcium channels and signal transduction pathways. J Cell Sci 1997;110:2915–24.
[70] Liao W, Wei F, Qian MX, Zhao XS. Characterization of protein immobilization on alkyl monolayer modified silicon(1 1 1) surface. Sensors Actuators B 2004;101:361–7.